Title
Estimation of stress and stress-induced permeability change in a geological nuclear waste repository in a thermo-hydrologically coupled simulation

Authors
Sasaki, Tsubasa
Rutqvist, Jonny

Publication Date
2021

DOI
10.1016/j.compgeo.2020.103866

Peer reviewed

Estimation of stress and stress-induced permeability change in a geological nuclear waste repository in a thermo-hydrologically coupled simulation

Abstract

Geologic disposal is a promising solution for a safe permanent isolation of accumulated high-level nuclear waste from nuclear powerplants. The behavior of host rock is highly coupled thermally, hydromechanically, and chemically. Numerical simulations of such coupled phenomena for the extremely long term (> 100,000 years) and large length scale (> 1 km) of geologic disposal remain to be computationally challenging. In this study, a methodology has been developed to approximate stress and stress-induced permeability change in host rock using only thermo-hydrological (TH) variables. A coupled thermo-hydromechanical (THM) simulation is carried out using TOUGH-FLAC simulator to model THM behaviors of a generic nuclear waste repository, in order to evaluate the performance of the developed methodology, which is implemented in a coupled TH simulation. Results show that stress and permeability change estimated by the developed methodology in the TH-coupled simulation match those calculated in the THM-coupled simulation over the simulated timeframe of over 10,000 years. Details about errors in stress and permeability estimates accrued by the developed methodology are discussed in this paper. The developed methodology will help incorporate stress-induced permeability change into existing TH simulators for the long-term radionuclide transport in geologic disposal.

1. Introduction

The United States has accumulated, as of end of 2018, over 84,000 metric tons of high-level nuclear waste [1], which must be stored remotely and carefully such that the waste will be permanently isolated from human beings and the biosphere [2]. Geological disposal is considered for safe permanent isolation of high-level nuclear waste, and hence such possibility is being extensively investigated in many countries considering various host rocks [3], including the past studies at the Yucca Mountain, Nevada, USA [4]. For each deep disposal site, the safety is to be assessed on the basis of a safety case developed from the scientific and technical basis for geological disposal [5]. The core of the safety case consists of safety and performance assessments. In a safety assessment, the estimated consequences of any releases from the repository are compared with the appropriate safety criteria, whereas in a performance assessment (PA), the evolution and performance of the isolation barriers for hundreds of thousands of years is estimated [6].

One type of host rock formations considered for geologic nuclear waste disposal is clay/shale formations, because of their favorable properties (e.g., low permeability, slow diffusion, high retention of radionuclides, self-healing of fractures) to curtail migration of radionuclides if released from a waste package. As a result, many studies have been conducted to assess the feasibility of nuclear waste storage in clay/shale formations in Europe [7]–[10] as well as in the US [11], [12]. Another feature of clay/shale formation is their relatively low thermal conductivity, which maybe a disadvantage because it can lead to high temperatures that need to be managed by, for example, storing the waste for a long time on the surface before underground disposal.

In the US, the properties of clay/shale formations are currently being investigated as potential feasible host rock formations for nuclear waste disposal [13] and generic (non-site specific) PA model simulations are developed and tested [14]. PFLOTRAN [15] is a state-of-the-art massively parallel subsurface flow and reactive transport code that is being applied for such PA modeling exercises. However, PA calculations with uncertainty quantification will require a large number of simulations, while at the same time need to consider the evolution of the system over hundreds of thousands of years. This includes potential changes in the transport properties, such as the permeability of host rock, induced by coupled thermo-hydro-mechanical-chemical (THMC) processes.

Field experiments at underground rock laboratories as well as numerical simulation have shown that strongly coupled THM processes is likely to occur in a clay/shale repository [16]–[19] that could also be impacted by chemical processes [20], [21]. For example, so-called thermal pressurization and thermal stress could potentially lead to formation fracturing or shear activation, as well as high stress concentration and damage around emplacement tunnels (Figure 1) [22]. Moreover, increasing horizontal stress will act on the repository tunnels and that, through stress concentration around the tunnel openings, could cause compressive spalling failure or tensile failure in different parts of the tunnel walls (Figure 1).

Stresses and potential failure around tunnel openings will impact the formation and evolution of the disturbed zone around the emplacement tunnels. Generally, the disturbance may be divided into excavation disturbed (EdZ) and damaged zones (EDZ). The EdZ is a zone with hydro-mechanical and geochemical modifications, without major changes in flow and transport properties, whereas the EDZ is a zone with hydro-mechanical and geochemical modifications, inducing significant changes in flow and transport properties [23]. The THM evolution within the bentonite buffer will also impact the EDZ evolution as the re-saturation and swelling of the bentonite buffer provides mechanical support to the EDZ [19]. In turn, the swelling pressure may be affected by chemical changes within the bentonite buffer, thus leading to the necessity for such coupled THMC evolution to be assessed over the regulatory repository period [20].

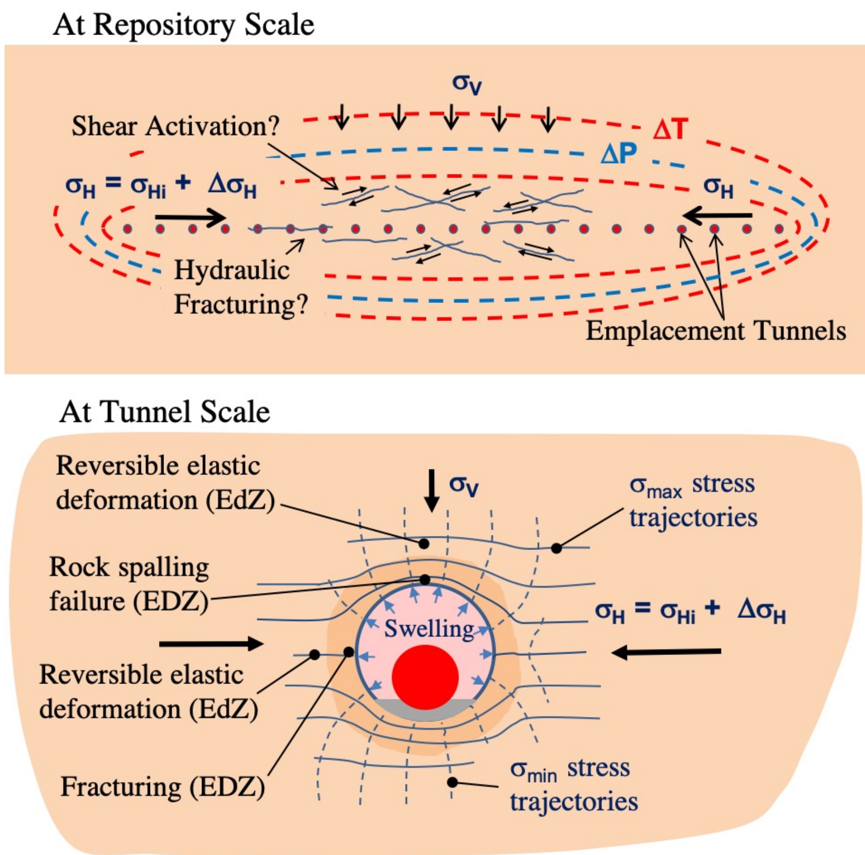

Figure 1 Schematic of repository scale coupled thermo-hydro-mechanical responses and their impact on emplacement tunnels (Modified from Rutqvist, 2020).

Coupled THMC numerical analyses are computationally challenging considering the extremely long timeframe that is required for geological disposal, which is beyond hundreds of thousands of years, in addition to the spatial and temporal resolutions required to sufficiently resolve the geomechanics. Among the THMC processes, the mechanical part is often the most time-consuming as complex constitutive equations must be solved to simulate elasto-plastic and failure response of the rock as well as of the buffer material filled between the rock and nuclear waste canister. Hence, there is a need for a method which can approximate the mechanical behavior of the repository and its effect on flow properties of the rock (i.e., permeability) from thermal, hydrological, and/or chemical behaviors of the repository. Such a method is beneficial for existing radionuclide transport simulators, such as PFLOTRAN, which are usually only thermo-hydrologically (TH) coupled with radionuclide transport, as mechanically-induced permeability change can be incorporated so as to improve the accuracy of the radionuclide flow simulation.

In this study, a coupled THM simulation is conducted to model the behavior of a generic clay/shale geological repository for nuclear waste. A method to approximate the mechanical response of the repository is then developed which only requires TH variables to estimate stress and stress-induced permeability change. The performance of the approximation method is evaluated in comparison between the coupled THM and TH simulations in calculating stress and stress-induced permeability change in the rock as well as in the buffer during heating from the nuclear waste canister. The objectives of this study are as follows:

- Estimate stress and stress induced-permeability change in a generic clay/shale geological repository for nuclear waste in the long term
- Develop a methodology to approximate the mechanical response of the rock and buffer around the nuclear waste canister from TH variables

TOUGH-FLAC simulator (Rutqvist, 2011; Rinaldi et al., 2018; Luu, 2020) is employed to model THM behaviors of the generic nuclear waste repository. Recent TOUGH-FLAC versions consist of the newly updated TOUGH3 multiphase fluid and thermal transport code [25] and the commercial FLAC3D code [26], in which TOUGH3 is the master code (Blanco-Martín et al., 2016; Kim et al., 2011; Rinaldi et al., 2018). TOUGH3 solves the thermo-hydrological equations and passes TH variables (i.e., pore pressure, gas saturation, capillary pressure, and temperature in the case of equation of state #4 (EOS4)) to FLAC3D at each converged TOUGH3 time step. FLAC3D is then called to solve the mechanical equations under drained conditions to calculate stresses, which are then used to update TH variables and parameters in TOUGH3 (i.e., permeability, porosity, and capillary pressure). A TOUGH-FLAC simulation runs in this sequential manner to model various THM coupled phenomena in geological formation [19], [29], [30]. The Barcelona Basic Model (BBM) [31] is used to simulate the mechanical response of the buffer, which is assumed to be composed of swelling bentonite. In the following section, further details about the methodology of this study are provided.

2. Methods

2.1 Model geometry

Figure 2 shows the geometry and mesh of the generic nuclear waste repository. The nuclear waste disposal tunnel is located at the center of the model, which is at the depth of 500 m from the ground surface and 25 m away horizontally from the lateral boundaries (i.e., mid-pillar). The inner and outer radii of the canister are 0.35 m and 0.45 m, respectively, whereas the radius of the tunnel is 1.14 m. This model is three dimensional but the plane-strain condition is applied in the out-of-plane direction where the model thickness is 1 m. The entire model is discretized into 360 elements (i.e., 248 for the rock, 96 for the buffer, and 16 for the canister) and the size of the mesh is set finer around the center of the tunnel than the rest of the model domain.

Boundary conditions are also shown in Figure 2. Thermo-hydrological boundary conditions are set as follows: constant pore pressure and temperature on the top and bottom boundaries, and no fluid flow or heat flux along the lateral and canister interior boundaries. A time-varying heat source (Figure 3) is prescribed in each of the sixteen canister elements to model the heat flux from the nuclear waste package. Mechanical boundary conditions are set as follows: zero displacement perpendicular to the bottom and lateral boundaries (displacement parallel to the boundary surfaces is allowed) and in the out-of-plane direction, and constant pressure on the top and canister interior boundaries. The model geometry and boundary conditions are to represent conditions and THM evolution for an emplacement tunnel at the inner part of a repository, where the highest temperature changes and thermal impact could be expected due to symmetry assumptions at the tunnel scale (Figure 1).

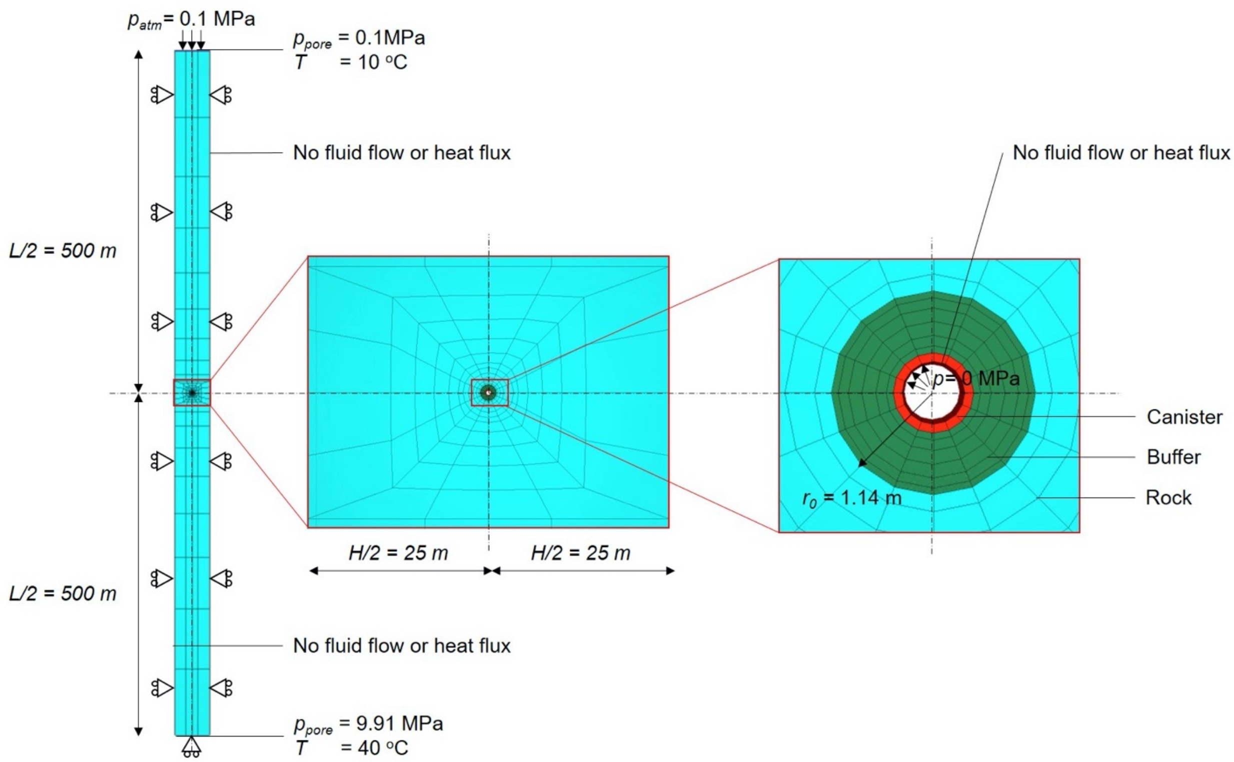

Figure 2 The geometry and mesh of the generic nuclear waste repository model.

2.2 Material behaviors

2.2.1 Thermo-hydrological behaviors

The thermo-hydrological (TH) behaviors of the model are computed by the TOUGH3 simulator. The equation-of-state module #4 (EOS4) is used. In EOS4, the model components are water and air, which can be either in the gas or liquid phase, and the primary variables are gas pressure, gas saturation, and air partial pressure for two-phase conditions, whereas they are gas pressure, temperature, and air partial pressure for single-phase conditions.

Darcy's law is used to simulate the multiphase flow of the fluid components, which is expressed as follows:

$$q_i = -\frac{k_{ri}k}{\mu_i}\nabla P_i \tag{1}$$

where q_i is the flow rate, k_{ri} is the relative permeability, k is the absolute permeability, μ_i is the dynamic viscosity, and ∇P_i is the pressure gradient. The subscript *i* indicates that the parameters are for phase *i*. The following relative permeability function (i.e., van Genuchten-Mualem model) is used for the rock:

$$k_{rl} = \begin{cases} \sqrt{S^*}\left(1-\left(1-(S^*)^{\frac{1}{\lambda_k}}\right)^{\lambda_k}\right)^2 & if\ S_l < S_{ls} \\ 1 & if\ S_l \geq S_{ls} \end{cases}$$

$$k_{rg} = \begin{cases} 1-k_{rl} & if\ S_{gr} = 0 \\ (1-\hat{S})^2\left(1-\hat{S}^2\right) & if\ S_{gr} > 0 \end{cases} \tag{2}$$

where

$$S^* = \frac{S_l - S_{lr}}{S_{ls} - S_{lr}} \tag{3}$$

$$\hat{S} = \frac{S_l - S_{lr}}{1 - S_{lr} - S_{gr}} \tag{4}$$

where k_{rl} is relative permeability of the liquid phase, k_{rg} is relative permeability of the gas phase, λ_k is a van Genuchten parameter (in the original notation [32] λ_k is expressed as m), S_l is liquid phase saturation, S_{lr} is residual (i.e., minimum) liquid phase saturation, S_{ls} is saturated (i.e., maximum) liquid phase saturation, and S_{gr} is residual gas phase saturation. It is noted that $0 \leq k_{rl} \leq 1$ and $0 \leq k_{rg} \leq 1$ are imposed.

The following relative permeability function is used for the bentonite buffer:

$$\begin{aligned} k_{rl} &= \hat{S}^3 \\ k_{rg} &= 1 \end{aligned} \tag{5}$$

As to the calculation of capillary pressure, the following equation (i.e., van Genuchten model) is used for both rock and bentonite buffer:

$$P_{cap} = -P_0 \left((S^*)^{\frac{-1}{\lambda_k}} - 1 \right)^{1-\lambda_k} \tag{6}$$

where P_0 is a parameter analogous to the air entry pressure. The maximum capillary pressure value, P_{max}, is specified such that $-P_{max} \leq P_{cap} \leq 0$.

Fourier's law and Fick's law are used to simulate thermal conduction and multi-phase diffusion, respectively.

Table 1 shows the TH parameter values (i.e., TOUGH3 input parameter values) employed in this study for the rock, buffer, and canister. It is noted that the residual liquid saturation value for the capillary pressure function is set smaller than that for the relative permeability function. This is done so as to avoid incurring infinite capillary pressure values when the liquid phase becomes immobile. In addition, all phases are assumed perfectly mobile ($k_{rl} = k_{rg} = 1$) in the canister and identical capillary pressure function and parameter values that are employed for the buffer are used for the canister. This is done to alleviate convergence issues for the flow calculation at the buffer-canister interface. The hydrological behavior of the buffer would not be erroneously affected by that of the canister as the porosity of the canister is set to a value significantly smaller than that of the rest of the rock and bentonite buffer. The inside part of the canister, where nuclear waste is supposed to be stored, is ignored in the model as such part would not have mechanical resistance or affect fluid flow or heat flux calculations as long as an equivalent heat source is assigned to the canister elements. The canister elements are treated as a porous medium due to the requirements of TOUGH3. The porosity of the canister elements is set to a value that is orders of magnitude smaller than that of the bentonite and rock, in order to mitigate the inconsistency.

Table 1 Thermo-hydrological parameter values of the model.

	Rock	Buffer	Canister
Grain density (kg/m^3)	2700	2700	7800
Porosity (-)	0.15	0.41	0.001
Absolute permeability (m^2)	$5 \cdot 10^{-20}$	$2 \cdot 10^{-21}$	$2 \cdot 10^{-21}$
Thermal conductivity (W/(m·°C))	2.2	1.26	12.0

Grain specific heat (J/(kg·°C))	900	800	500
Pore compressibility (1/Pa)	$1\cdot10^{-9}$	$5\cdot10^{-8}$	0
Pore expansivity (1/°C)	0	$1\cdot10^{-4}$	0
Diffusion coefficient for water vapor (m^2/s)	$1.73\cdot10^{-5}$	$1.73\cdot10^{-5}$	$1.73\cdot10^{-5}$
van Genuchten parameter, λ_k (-)	0.41	0.32	0.32
Residual liquid saturation for relative permeability, S_{lr} (-)	0.2	-	-
Residual liquid saturation for capillary pressure, S_{lr} (-)	0.1	0.1	0.1
Saturated liquid saturation, S_{ls} (-)	1.0	1.0	1
Residual gas saturation, S_{gr} (-)	0.01	0	0
Capillary pressure parameter, P_0 (Pa)	$4.76\cdot10^{7}$	$3\cdot10^{7}$	$3\cdot10^{7}$
Maximum capillary pressure, P_{max} (Pa)	$1\cdot10^{8}$	$5\cdot10^{9}$	$5\cdot10^{9}$

2.2.2 Mechanical behaviors

The mechanical behavior is modelled by the FLAC3D simulator in the THM coupled simulation case, whereas they are modelled analytically in the TH coupled simulation case, which will be explained in detail in later sections. In either case, the stress-strain relation (i.e., constitutive model) is described in terms of the effective stress, which is defined as follows:

$$\begin{aligned} \sigma_{ij}^{'} &= \sigma_{ij} - \alpha_{BW} \cdot p_{pore}\delta_{ij} \\ p_{pore} &= max\left(p_g, p_l\right) \end{aligned} \tag{7}$$

where σ'_{ij} is the effective stress (tensor), σ_{ij} is the total stress (tensor), α_{BW} is the Biot-Willis coefficient, δ_{ij} is the Kronecker delta, p_{pore} is pore pressure, p_g is gas phase pressure, and p_l is the liquid phase pressure. If the pore space is fully saturated with the liquid phase (i.e., water), pore pressure is the liquid phase pressure, whereas it is the gas phase pressure if the pore space is partially saturated.

The linear isotropic elastic constitutive relation is used to model the mechanical behavior of the rock and canister, where only two elastic parameters (e.g., Young's modulus and Poisson's ratio) are required.

The Barcelona Basic Model (BBM) [31] is used to model the mechanical behavior of the bentonite buffer. This model is effective in simulating the stress and strain change of swelling clays during monotonic saturation/desaturation, which is expected to occur in the bentonite buffer. The elastic mechanical behavior of the BBM is nonlinear and plastic yielding and plastic hardening/softening are included. More advanced models [33], [34] are available in case the stress and strain change during cyclic saturation/desaturation needs to be simulated. The mechanical parameter values used for the model are listed in Table 2.

Table 2 Mechanical parameter values of the model.

	Rock	Buffer	Canister
Young's modulus (Pa)	$5.0 \cdot 10^{9}$	-	$200 \cdot 10^{9}$
Poisson's ratio (-)	0.3	0.4	0.3
Biot-Willis coefficient, α_{BW} (-)	1.0	1.0	1.0
Linear thermal expansion coefficient (1/°C)	$1.0 \cdot 10^{-5}$	$1.5 \cdot 10^{-4}$	$1.0 \cdot 10^{-5}$
Gradient of swelling line for stress, κ_{PS0} (-)	-	0.05	-
Gradient of swelling line for suction, κ_{SP0} (-)	-	0.25	-

Swelling gradient adjusting parameter, α_{PS} (1/Pa)	-	$-3.0\cdot10^{-9}$	-
Swelling gradient adjusting parameter, α_{SS} (1/Pa)	-	0	-
Swelling gradient adjusting parameter, α_{SP} (-)	-	-0.161	-
Reference pressure, p_{ref} (Pa)	-	$0.01\cdot10^{6}$	-
Gradient of compression line for stress, λ_{PS0} (-)	-	0.15	-
Gradient of compression line for suction, λ_{SP0} (-)	-	0.5	-
Compression gradient adjusting parameter, r_λ (-)	-	0.925	-
Compression gradient adjusting parameter, β_λ (1/Pa)	-	$0.1\cdot10^{-6}$	-
Tensile strength at zero suction, p_{s0} (Pa)	-	0	-
Tensile strength gradient, k_s (-)	-	0.1	-
Tensile strength gradient adjusting parameter, ρ_s (1/^{o}C)	-	0	-
Reference mean net stress, p^c (Pa)	-	$0.5\cdot10^{6}$	-
Critical state frictional constant, M (-)	-	1.0	-
Pre-consolidation mean net stress, p_0^* (Pa)	-	$12.0\cdot10^{6}$	-
Porosity (-)	-	0.41	-
Non-associated plastic flow parameter, α_a (-)	-	0.53	-

2.3 Simulation stages

2.3.1 In situ conditions

The in situ conditions of the model prior to the excavation of the nuclear waste disposal tunnel are specified as follows: the temperature is linearly increased with depth from 10^{o}C on the top boundary to 40^{o}C on the bottom boundary, and pore pressure and stresses are also linearly increased with gradients corresponding to the weight of pore water and rock, respectively. The in situ rock stresses are assumed either isotropic or anisotropic in this study, which are explained in detail in later sections. At the in situ state, the volume inside the tunnel is occupied by rock elements while the buffer and canister elements are deactivated.

2.3.2 Tunnel excavation stage

The TH part of the tunnel excavation stage is simulated by TOUGH3 as follows: constant pore pressure of 0.1 MPa and constant temperature of 25ºC are specified in the buffer and canister elements and the TOUGH3 simulation is run for 1.5 years. The pore pressure and temperature profiles at the end of the simulated timeframe are used as the initial pore pressure (p_{pore0}) and temperature (T_0) in the following canister heating stage.

The mechanical part of the tunnel excavation stage is simulated by FLAC3D as follows: first the stiffness of the buffer and canister elements is set to small values (smaller by orders of magnitudes than that of the rock) so as not to restrict the displacement of the tunnel boundary, and then pore pressure and temperature values at each converged TOUGH3 time step are imported and used as boundary conditions in FLAC3D to compute the corresponding displacements, strains, and stresses. The stress distributions at the end of the 1.5-year simulation timeframe are used as the initial stress values for the THM simulation case of the canister heating stage. For the TH simulation case, on the other hand, the initial stresses after tunnel excavation are calculated analytically as described in a later section.

2.3.3 Canister heating stage

The canister heating stage is simulated by introducing a time-varying heat source in the canister elements in TOUGH3. Figure 3 shows the heat rate assigned to the canister elements. The power curve shown in Figure 3 corresponds to a 4-PWRelement waste package which is assumed to be emplaced after 60 years of interim storage with the center-to-center spacing of 9 m between individual waste canisters along the tunnel axis. The initial power is specified as 200 (W/m) where the unit W/m means power per unit length along the axis of the tunnel. The power is divided by the number of the canister elements (i.e., sixteen), which renders the initial power of 12.5 (W/m) for each canister element as shown in Figure 3. Also, the mechanical parameter values of the buffer and canister are changed from the fictitious values used in the excavation stage to the ones listed in Table 2. The initial stresses in the buffer and canister are set as follows: $\sigma_{xx} = \sigma_{yy} = \sigma_{zz} = 0.15$ MPa (compression positive) and $\tau_{xx} = \tau_{yy} = \tau_{zz} = 0$ MPa. The initial pore pressure (gas pressure) and temperature in the buffer and canister are set to 0.1 MPa and 25°C. Finally, the initial liquid phase saturation in the buffer and canister is set to 0.65. The canister heating stage is simulated up to 100,000 years.

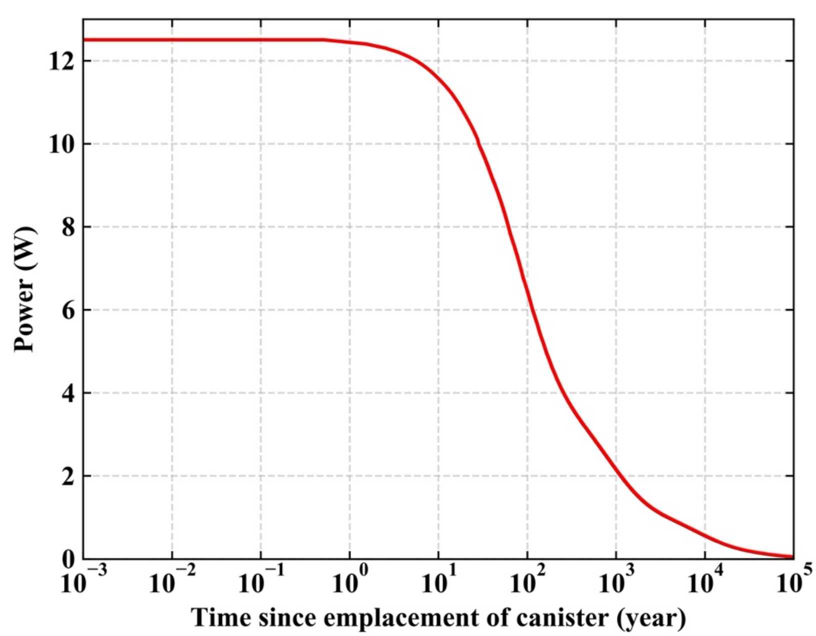

Figure 3 Heat rate assigned to the canister elements.

2.4 Stress calculation methodologies

2.4.1 Stress approximation using TH variables

In this section, a methodology is developed to estimate stresses from TH variables, such as pore pressure (i.e., gas pressure), temperature, and suction (i.e., the absolute value of capillary pressure). The stress estimates can then be used to calculate stress-induced permeability changes. It is noted that compressive stress is expressed in positive values in the following derivation of the stresses.

2.4.1.1 Buffer stresses

The buffer stress in the direction normal to the tunnel surface, p_B, is calculated by the Barcelona Basic Model (BBM) under the assumption that the volume of the buffer (i.e., the space in between the canister and the waste disposal tunnel) remains constant ($d\epsilon_{total} = d\epsilon_{mechanical} + d\epsilon_{suction} + d\epsilon_{thermal} = 0$) and that the strain increments are isotropic (no shear components). The stress-strain relation of BBM is nonlinear, hence the buffer stress has to be calculated iteratively as follows:

$$
\begin{aligned}
p'_{B,i+1} &= p'_{B,i} + \Delta p'_{B,i} \\
\Delta p'_{B,i} &= K'_i\left(\Delta\epsilon_{s,i} + \Delta\epsilon_{th,i}\right)
\end{aligned}
\qquad (8)
$$

where p'_B is the mean effective stress in the buffer, $\Delta p'_B$ is the mean effective stress increment in the buffer, K' is the bulk modulus of the buffer, $\Delta\epsilon_s$ is the suction-induced volumetric strain increment, and $\Delta\epsilon_{th}$ is the thermally-induced volumetric strain increment. The subscript $_i$ indicates the step number. The bulk modulus and strain increments are calculated as follows:

$$K_i' = \frac{\upsilon p_{B,i}'}{\kappa_{PS,i}} \tag{9}$$

$$\Delta\epsilon_{s,i} = \frac{-\kappa_{SP,i}}{\upsilon(s_i + p_{atm})}\left(s_{B,i+1} - s_{B,i}\right) \tag{10}$$

$$\Delta\epsilon_{th,i} = 3\alpha_B\left(T_{B,i+1} - T_{B,i}\right) \tag{11}$$

where υ is specific volume of the buffer, κ_{PS} is a stiffness coefficient of the buffer against mean effective stress change, κ_{SP} is a stiffness coefficient of the buffer against suction change, p_{atm} is the atmospheric pressure, s_B is suction in the buffer (i.e., the absolute value of capillary pressure), α_B is the linear thermal expansion coefficient of the buffer, and T_B is temperature in the buffer. The stiffness coefficients are suction- and/or mean effective stress-dependent as shown below:

$$\kappa_{PS,i} = \kappa_{PS0}\left(1 + \alpha_{PS} s_{B,i}\right) \tag{12}$$

$$\kappa_{SP,i} = \kappa_{SP0}\left(1 + \alpha_{SP} \ln\frac{p_{B,i}'}{p_{ref}}\right)\exp\left(\alpha_{SS} s_{B,i}\right) \tag{13}$$

where κ_{PS0} is the stiffness coefficient against mean effective stress change at zero suction, κ_{SP0} is the stiffness coefficient against suction change at zero mean effective stress and zero suction, p_{ref} is a reference pressure value, and α_{PS}, α_{SP}, α_{SS} are stiffness-adjusting parameters.

Finally, the mean total stress in the buffer (i.e., buffer stress in the direction normal to the tunnel surface) is obtained as follows:

$$p_{B,i} = p_{B,i}^{'} + p_{pore,\,i} \tag{14}$$

where p_{pore} is pore pressure in the buffer.

2.4.1.2 Rock stresses

In order to calculate stresses in the formation around the nuclear waste storage tunnel, Kirsch equations are utilized under the analytical model domain and boundary conditions assumed as shown in **Error! Reference source not found.**. The horizontal displacement on the lateral boundaries are restricted while constant pressure loads, whose magnitude corresponds to the vertical total stress level at the depth of the tunnel, are specified on the top and bottom boundaries. The gravity is ignored in mechanical calculations (but not in thermo-hydraulic calculations) in the model domain. The vertical length of the model is arbitrary but it should be sufficiently larger than the diameter of the tunnel and on the same order as the horizontal length of the model.

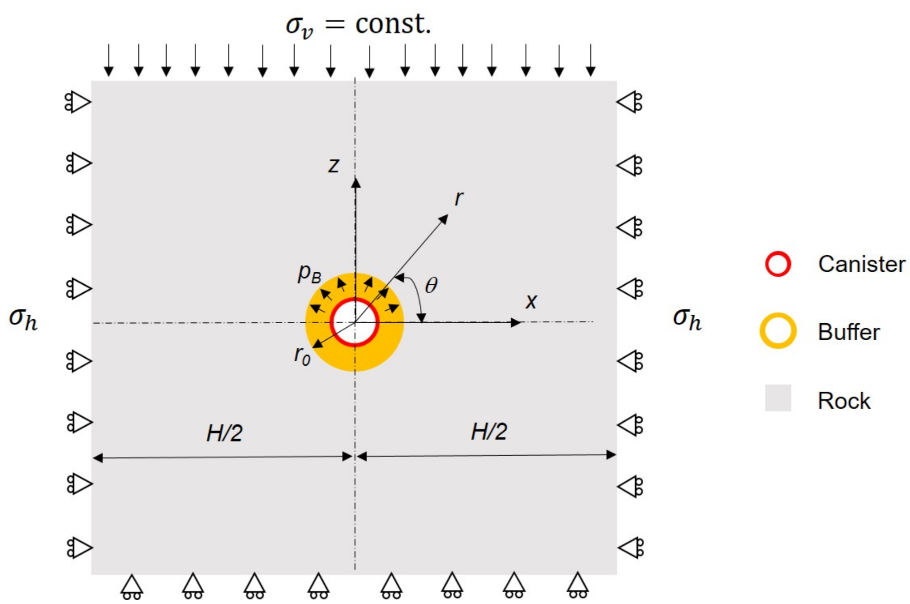

Figure 4 Analytical model of the proximity of the nuclear waste disposal tunnel.

The total stress on the lateral boundary (i.e., mid-pillar) after the emplacement of the canister is calculated from Hooke's law for linear isotropic elastic material under the plane-strain ($d\epsilon_{H,total} = d\epsilon_{H,mech} + d\epsilon_{H,thermal} = 0$) and zero-lateral strain ($d\epsilon_{h,total} = d\epsilon_{h,mech} + d\epsilon_{h,thermal} = 0$) conditions as follows:

$$\sigma_h = \frac{2\mu}{\lambda + 2\mu}\left(p_{pore}\Big|_{r=\frac{H}{2},\theta=0} - p_{pore0}\Big|_{r=\frac{H}{2},\theta=0}\right) + \frac{3\lambda\mu + 2\mu^2}{\lambda + 2\mu} 2\alpha\left(T\Big|_{r=\frac{H}{2},\theta=0} - T_0\Big|_{r=\frac{H}{2},\theta=0}\right) + \sigma_{h0} \tag{15}$$

where σ_h is the lateral boundary stress, p_{pore} is pore pressure, T is temperature, σ_{h0}, p_{pore0}, and T_0 are the initial lateral boundary stress, pore pressure and temperature, respectively, at the start of the canister heating stage, α is the linear thermal expansion coefficient of the rock. The subscript $\Big|_{r=\frac{H}{2},\theta=0}$ indicates the specific location of the model from which the pore pressure and temperature values are extracted to be substituted in the equation. The definitions of r, θ, H are provided in Figure 4. The parameter λ and μ are the Lamé constants, which are defined as follows:

$$\lambda = \frac{E\nu}{(1+\nu)(1-2\nu)}$$
$$\mu = \frac{E}{2(1+\nu)} \tag{16}$$

where E is Young's modulus and ν is Poisson's ratio. The radial and circumferential stresses in the rock are calculated from the Kirsch equations as follows:

$$\sigma_{rr} = \frac{\sigma_v + \sigma_h}{2}\left(1 - \left(\frac{r_0}{r}\right)^2\right) + \left(\frac{r_0}{r}\right)^2 p_B - \frac{\sigma_v - \sigma_h}{2}\left(1 - 4\left(\frac{r_0}{r}\right)^2 + 3\left(\frac{r_0}{r}\right)^4\right)\cos 2\theta \tag{17}$$

$$\begin{aligned}\sigma_{\theta\theta} &= \frac{\sigma_v + \sigma_h}{2}\left(1 + \left(\frac{r_0}{r}\right)^2\right) - \left(\frac{r_0}{r}\right)^2 p_B + \frac{\sigma_v - \sigma_h}{2}\left(1 + 3\left(\frac{r_0}{r}\right)^4\right)\cos 2\theta \\ &+ \frac{E\alpha\left(T - T\big|_{r=\frac{H}{2},\theta=0}\right)}{(1-\nu)} + \frac{E\left(p_{pore} - p_{pore}\big|_{r=\frac{H}{2},\theta=0}\right)}{3K(1-\nu)}\end{aligned} \tag{18}$$

$$\tau_{r\theta} = \frac{\sigma_v - \sigma_h}{2}\left(1 + 2\left(\frac{r_0}{r}\right)^2 - 3\left(\frac{r_0}{r}\right)^4\right)\sin 2\theta \tag{19}$$

where r_0 is the radius of the tunnel, and $\sigma_v = \rho_{rock} g L/2$ is the constant vertical stress (ρ_{rock} is the rock bulk density, and g is the gravitational acceleration). It is noted that the out-of-plane shear stresses

$(\tau_{ry}, \tau_{\theta y})$ are assumed to be negligible. The out-of-plane normal stress is calculated from Hooke's law for linear isotropic elastic material under the plane-strain condition ($d\epsilon_{yy,total} = d\epsilon_{yy,mech} + d\epsilon_{yy,thermal} = 0$) as follows:

$$\sigma_{yy} = \frac{\lambda}{2(\lambda+\mu)}\left((\sigma_{rr} - \sigma_{rr0}) + (\sigma_{\theta\theta} - \sigma_{\theta\theta 0}) - 2\left(p_{pore} - p_{pore0}\right) - 2\lambda\alpha(T - T_0)\right) + (\lambda + 2\mu)\alpha(T - T_0) + \left(\sigma_{yy0} - p_{pore0}\right) + p_{pore} \tag{20}$$

where p_{pore} is pore pressure, and T_0, p_{pore0}, σ_{rr0}, $\sigma_{\theta\theta 0}$, σ_{yy0} are the initial temperature, pore pressure, radial stress, circumferential stress, and out-of-plane stress, respectively, at the start of the canister heating stage.

The initial stresses $(\sigma_{h0}, \sigma_{rr0}, \sigma_{\theta\theta 0}, \tau_{r\theta 0}, \sigma_{yy0})$ are those after the excavation of the nuclear waste disposal tunnel, which are calculated as follows:

$$\sigma_{h0} = \frac{2\mu}{\lambda + 2\mu}\left(p_{pore0}\Big|_{r=\frac{H}{2},\theta=0} - p_{pore,in\ situ}\Big|_{r=\frac{H}{2},\theta=0}\right) + \frac{3\lambda\mu + 2\mu^2}{\lambda + 2\mu} 2\alpha\left(T_0\Big|_{r=\frac{H}{2},\theta=0} - T_{in\ situ}\Big|_{r=\frac{H}{2},\theta=0}\right) + \sigma_{h,in\ situ} \tag{21}$$

$$\sigma_{rr0} = \frac{\sigma_v + \sigma_{h0}}{2}\left(1 - \left(\frac{r_0}{r}\right)^2\right) + \left(\frac{r_0}{r}\right)^2 p_{tunnel} - \frac{\sigma_v - \sigma_{h0}}{2}\left(1 - 4\left(\frac{r_0}{r}\right)^2 + 3\left(\frac{r_0}{r}\right)^4\right)\cos 2\theta \tag{22}$$

$$\sigma_{\theta\theta} = \frac{\sigma_v + \sigma_{h0}}{2}\left(1 + \left(\frac{r_0}{r}\right)^2\right) - \left(\frac{r_0}{r}\right)^2 p_{tunnel} + \frac{\sigma_v - \sigma_{h0}}{2}\left(1 + 3\left(\frac{r_0}{r}\right)^4\right)\cos 2\theta + \frac{E\alpha\left(T_0 - T_0\big|_{r=\frac{H}{2},\theta=0}\right)}{(1-\nu)} + \frac{E\left(p_{pore0} - p_{pore0}\big|_{r=\frac{H}{2},\theta=0}\right)}{3K(1-\nu)} \tag{23}$$

$$\tau_{r\theta0} = \frac{\sigma_v - \sigma_{h0}}{2}\left(1 + 2\left(\frac{r_0}{r}\right)^2 - 3\left(\frac{r_0}{r}\right)^4\right)\sin 2\theta \tag{24}$$

$$\sigma_{yy0} = \frac{\lambda}{2(\lambda+\mu)}\Big(\left(\sigma_{rr0} - \sigma_{rr,in\,situ}\right) + \left(\sigma_{\theta\theta0} - \sigma_{\theta\theta,in\,situ}\right) - 2\left(p_{pore0} - p_{pore,in\,situ}\right) - 2\lambda\alpha\left(T_0 - T_{in\,situ}\right)\Big) + (\lambda + 2\mu)\alpha\left(T_0 - T_{in\,situ}\right) + \left(\sigma_{yy,in\,situ} - p_{pore,in\,situ}\right) + p_{pore0} \tag{25}$$

where p_{tunnel} is the (atmospheric) pressure inside the tunnel, and the subscript $_{in\ situ}$ indicates the in situ (i.e., hydrostatic, geostatic) state prior to the excavation of the disposal tunnel. The in situ stresses are calculated as follows:

$$\begin{pmatrix} \sigma_{rr,in\,situ} \\ \sigma_{\theta\theta,in\,situ} \\ \tau_{r\theta,in\,situ} \\ \sigma_{yy,in\,situ} \end{pmatrix} = \begin{pmatrix} \sigma_{xx}\cos^2\theta + \sigma_{zz}\sin^2\theta \\ \sigma_{xx}\sin^2\theta + \sigma_{zz}\cos^2\theta \\ (-\sigma_{xx} + \sigma_{zz})\sin\theta\cos\theta + \tau_{xz} \\ \sigma_{yy} \end{pmatrix} \tag{26}$$

where

$$\begin{pmatrix} \sigma_{xx} \\ \sigma_{zz} \\ \tau_{xz} \\ \sigma_{yy} \end{pmatrix} = \begin{pmatrix} K_0\left(\rho_{rock} \cdot g \cdot (L/2 - z) - p_{pore,in\,situ}\right) + p_{pore,in\,situ} \\ \rho_{rock} \cdot g \cdot (L/2 - z) \\ 0 \\ K_0\left(\rho_{rock} \cdot g \cdot (L/2 - z) - p_{pore,in\,situ}\right) + p_{pore,in\,situ} \end{pmatrix} \tag{27}$$

where ρ_{rock} is the bulk density of rock, g is the gravitational acceleration, z is the vertical distance from the center of the tunnel (upward is positive), $L/2$ is the depth from the ground surface to the center of the tunnel, and K_0 is the lateral earth pressure coefficient. The out-of-plane shear stresses (τ_{xy}, τ_{yz}) are assumed to be nonexistent. It is noted that $\sigma_{h,in\,situ}$ is assumed equal to σ_{xx} at the depth of the center of the tunnel as shown below:

$$\sigma_{h,in\,situ} = K_0\left(\rho_{rock} \cdot g \cdot (L/2) - p_{pore,in\,situ}\right) + p_{pore,in\,situ} \tag{28}$$

The in situ (i.e., hydrostatic) pore pressure and (i.e., thermostatic) temperature prior to the tunnel excavation stage are calculated as follows:

$$p_{pore,in\ situ} = \rho_{water} \cdot g \cdot (L/2 - z) \tag{29}$$

$$T_{in\ situ} = \frac{T_{bottom} - T_{top}}{L} (L/2 - z) + T_{top} \tag{30}$$

where ρ_{water} is the density of pore water, and T_{top} and T_{bottom} are the static temperature at $z = \frac{L}{2}, -\frac{L}{2}$, respectively.

2.4.2 Stress calculation using THM coupling

The THM coupled simulation is implemented by the TOUGH-FLAC simulator, in order to evaluate the accuracy of stresses estimated by the TH stress approximation method introduced earlier. In this THM coupled stress calculation method, the stresses are calculated numerically by FLAC3D.

2.5 Simulation cases

2.5.1 Isotropic rock stress case

In this simulation case, in situ rock stresses prior to the tunnel excavation stage are assumed isotropic as shown in the equation below:

$$\sigma'_{xx} = \sigma'_{yy} = \sigma'_{zz} = (\rho_{rock} - \rho_{water}) g (L/2 - z) \tag{31}$$

where $\sigma'_{xx}, \sigma'_{yy}, \sigma'_{zz}$ are the effective stresses in the horizontal, out-of-plane, and vertical directions of the model, respectively, ρ_{rock} is the rock bulk density, ρ_{water} is the water bulk density, g is the gravitational acceleration, and z is the vertical distance from the center of the tunnel. The shear stresses are assumed nonexistent. The rock stresses are assumed isotropic because the modelled nuclear waste repository is generic (no specific site is intended). The objective of this study is to demonstrate the effectiveness of the stress approximation method using TH variables, and hence the in situ rock stresses are assumed the simplest in this baseline simulation case. More realistic rock stresses (i.e., anisotropic rock stresses) are considered in the following simulation case described below.

2.5.2 Anisotropic rock stress case

The anisotropic stress state of the clay/shale formation is referred from Mont Terri Rock Laboratory in Switzerland [35]. The rock at Mont Terri Rock Laboratory consists of the Opalinus Clay, which is one of the most ideal materials for nuclear waste repositories due to its extremely low permeability. A gallery tunnel at Mont Terri was excavated in 1998, which was located at the depth of roughly 250 m from the ground surface, in order to investigate the effect of excavation on the fracture development around the tunnel in the Opalinus Clay. The in situ stress state around the tunnel was measured by triaxial strain cells and the measurement indicated the following stress state: σ'_{xx} = -1.4 ~ 0.2 (MPa), σ'_{yy} = 2.0 (MPa), σ'_{zz} = 4.5 (MPa) [36], [37]. The horizontal stress estimate (σ'_{xx}) is uncertain because the tunnel was located in the vicinity of a valley. In this study, σ'_{xx} = 0.2 (MPa) is assumed. As a result, the lateral earth pressure coefficients are obtained as follows: $K_{0,yy} = \sigma'_{yy}/\sigma'_{zz} =$ 0.44, $K_{0,xx} = \sigma'_{xx}/\sigma'_{zz} =$ 0.044. The extrapolation of this stress state at Mont Terri to the generic repository model employed in this study is carried out as shown below:

$$
\begin{aligned}
\sigma'_{zz} &= (\rho_{rock} - \rho_{water})g(L/2 - z) \\
\sigma'_{xx} &= K_{0,xx}\sigma'_{zz} \\
\sigma'_{yy} &= K_{0,yy}\sigma'_{zz}
\end{aligned}
\tag{32}
$$

The shear stresses are assumed nonexistent. The above stresses are used as the in situ stress state for the anisotropic rock stress case.

2.6 Permeability profiles in rock near the tunnel

In this study, rock permeability near the disposal tunnel is calculated by the following equation:

$$k = \begin{cases} (k_r + \Delta k_{max} \exp\left(\beta_1 \sigma_m'\right)) \cdot \exp\left(\gamma \langle \sigma_d - \sigma_{d,crit} \rangle\right) & if\ r \leq 2r_0 \\ k_r & if\ r > 2r_0 \end{cases} \tag{33}$$

where k is the absolute permeability, Δk_{max} is the increment in absolute permeability due to mean effective stress change, β_1 (< 0) is a parameter correlating the absolute permeability and mean effective stress change, σ_m' is the mean effective stress (= mean total stress – pore pressure), γ (> 0) is a parameter correlating the absolute permeability and deviatoric stress change, σ_d is the deviatoric stress (= von Mises equivalent stress), and $\sigma_{d,crit}$ is the critical deviatoric stress value. The $\langle \quad \rangle$ operator is the MaCaulay brackets, in which $\langle x \rangle = x$ if $x \geq 0$ and $\langle x \rangle = 0$ if $x < 0$. The mean effective stress and deviatoric stress are defined as follows:

$$\sigma_m' = \frac{\sigma_{xx}' + \sigma_{yy}' + \sigma_{zz}'}{3} = \frac{\sigma_{rr}' + \sigma_{yy}' + \sigma_{\theta\theta}'}{3} \tag{34}$$

$$\sigma_d = \sqrt{\frac{1}{2}\left(\left(\sigma_{xx}-\sigma_{yy}\right)^2 + \left(\sigma_{yy}-\sigma_{zz}\right)^2 + (\sigma_{zz}-\sigma_{xx})^2 + 6\left(\tau_{xy}^2+\tau_{yz}^2+\tau_{xz}^2\right)\right)}$$
$$= \sqrt{\frac{1}{2}\left(\left(\sigma_{rr}-\sigma_{yy}\right)^2 + \left(\sigma_{yy}-\sigma_{\theta\theta}\right)^2 + (\sigma_{\theta\theta}-\sigma_{rr})^2 + 6\left(\tau_{ry}^2+\tau_{y\theta}^2+\tau_{r\theta}^2\right)\right)} \quad (35)$$

The excavation damaged zone (EDZ), where the permeability increases according to Equation 33, is assumed to be located within the area enclosed by twice the radius of the tunnel ($2r_0$). This size of EDZ is referred from experimental observations at Mont Terri Rock Laboratory [35]. Figure 5a and b show the absolute permeability profiles in the rock around the tunnel after the tunnel excavation stage for the isotropic and anisotropic rock stress cases, respectively. The permeability values are calculated with the parameter values listed in Table 3. The permeability increases near the tunnel due mainly to deviatoric stress increase for the isotropic rock stress case and to the combination of mean stress decrease and deviatoric stress increase for the anisotropic rock stress case. The size of EDZ is assumed constant in the canister heating stage.

Table 3 Parameter values for the rock permeability function.

Residual permeability, k_r (m^2)	$5\cdot10^{-20}$
Permeability increment, Δk_{max} (m^2)	$1\cdot10^{-17}$
Coefficient for mean effective stress, β_l (1/Pa)	$-1\cdot10^{-6}$
Coefficient for deviatoric stress, γ (1/Pa)	$3\cdot10^{-7}$
Critical deviatoric stress, $\sigma_{d,\ crit}$ (Pa)	$5\cdot10^{6}$

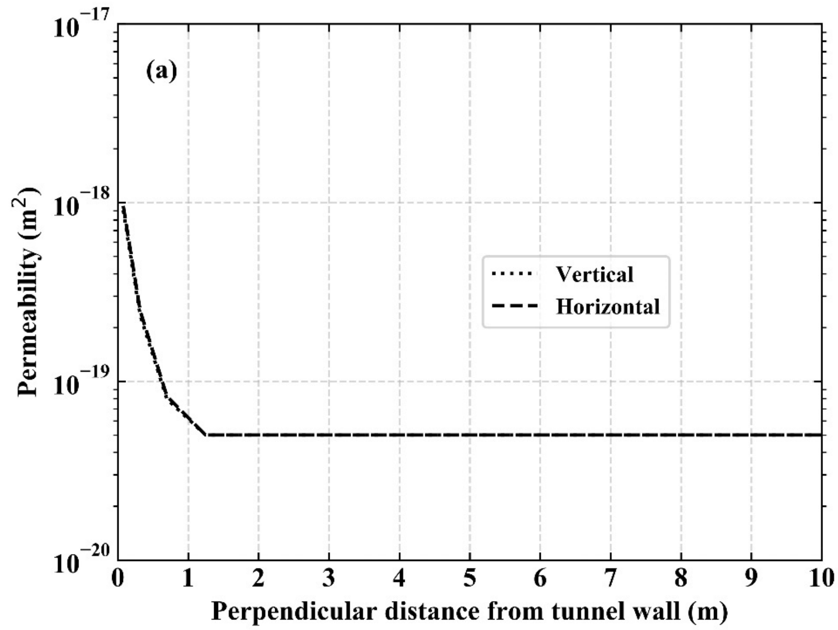

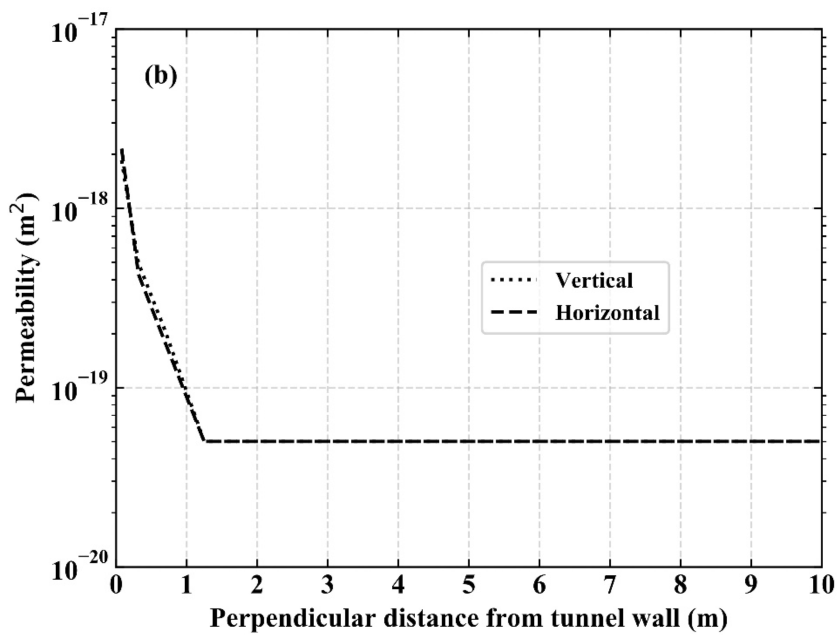

Figure 5 Absolute permeability profiles around the tunnel after excavation: (a) isotropic rock stress case; (b) anisotropic rock stress case.

3. Results

3.1 TH variables in the buffer

Figure 6 shows the evolution of TH variables (i.e., temperature, pore pressure, saturation, and capillary pressure) in the buffer during the canister heating stage. These time-varying profiles are taken from the buffer element located at the mid-thickness along the vertical axis ($r = 0.8$ m, $\theta = 90^{\circ}$).

Results are found identical between the TH and THM simulation cases (i.e., the solid (THM) and dashed (TH) lines are on top of each other), which indicates that the variance in stress-induced permeability change in the rock between the two cases has negligible effects on the fluid flow and heat transfer in the buffer. No difference is found between the isotropic and anisotropic rock stress cases either. Hence, only the result of the isotropic case is shown in Figure 6.

The maximum temperature in the buffer is approximately 85°C which is reached between 10 and 100 years since the canister emplacement. Around the same time, the buffer becomes fully saturated with water and pore pressure starts to increase significantly. Thermal expansion of the pore water (i.e., thermal pressurization) in the host rock causes the pore pressure buildup. Pore pressure still keeps increasing while temperature starts to decrease from its peak value at roughly 100 years. During this time, the pore pressure buildup is driven by the thermal pressurization of the surrounding rock, where the temperature peak occurs later than in the buffer due to slow heat transfer. Pore pressure peaks at slightly over 11 MPa, which is significantly greater than the hydrostatic pore pressure level of 4.5 MPa at this depth, and it starts to decrease when thermal depressurization starts to occur in the surrounding rock at approximately 1000 years.

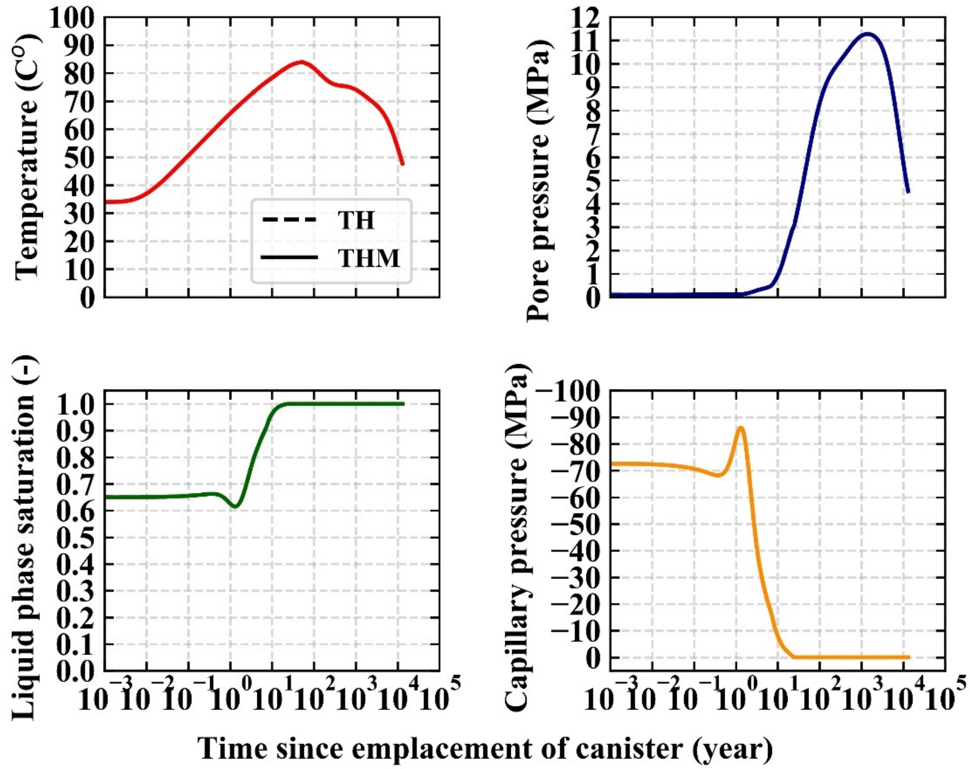

Figure 6 The evolution of TH variables (i.e., temperature, pore pressure, saturation, and capillary pressure) in the buffer during the canister heating stage.

3.2 Buffer stresses

Figure 7 shows the evolution of the mean total and effective stresses in the buffer during the canister heating stage (positive stress values indicate compression). The match between the TH and THM simulation cases is excellent, validating the stress approximation methodology developed for the TH simulation case. The mean effective stress change is driven by the suction-induced swelling, and hence it corresponds with the change in saturation (capillary pressure). Thermal expansion and contraction also contribute to the mean effective stress change but the impact of the thermal effect is secondary to that of the swelling effect. The peak total stress level of 15 MPa is reached at roughly 1000 years, which is slightly above the in situ total stress level at the tunnel depth before tunnel excavation. It is noted that no difference in the mean total and effective stress levels is calculated between the isotropic and anisotropic rock stress cases, hence only the result of the isotropic case is presented in Figure 7.

The deviation in buffer stress values between the TH and THM cases is caused primarily by the selection of buffer elements whose TH variables are used to calculate buffer stresses in the TH case. In this study, one buffer element at the mid-length in the thickness direction is chosen for simplicity reasons; averaging over two elements (one located by the tunnel wall and the other by the canister wall) did not improve the accuracy of buffer stress estimation. This is an acceptable simplification since radionuclide transport models (e.g., PFLOTRAN models) cannot usually afford fine meshing for the buffer (e.g., one or two elements in the thickness direction). Thus, selecting one buffer element for its TH variables to calculate buffer stresses is suitable.

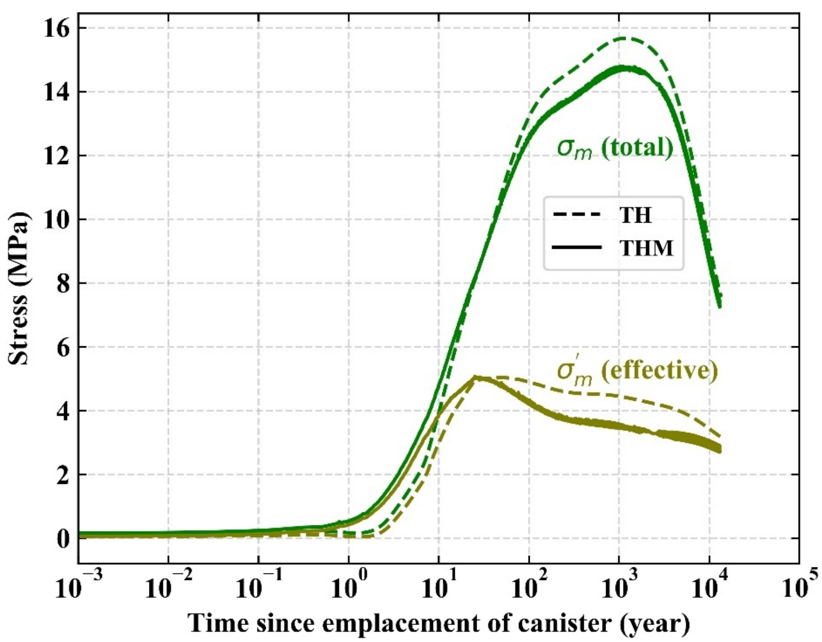

Figure 7 The mean total and effective stresse change in the buffer during the canister heating stage.

3.3 Rock stresses

Rock stresses (i.e., radial effective stress, σ'_{rr}, circumferential effective stress, $\sigma'_{\theta\theta}$, and out-of-plane effective stress, σ'_{yy}) are compared at eight different locations near the tunnel: four locations on the vertical axis (V1, V2, V3, V4) and the other four locations on the horizontal axis (H1, H2, H3, H4). These locations are shown in Figure 8. It is noted that positive stress values indicate compression.

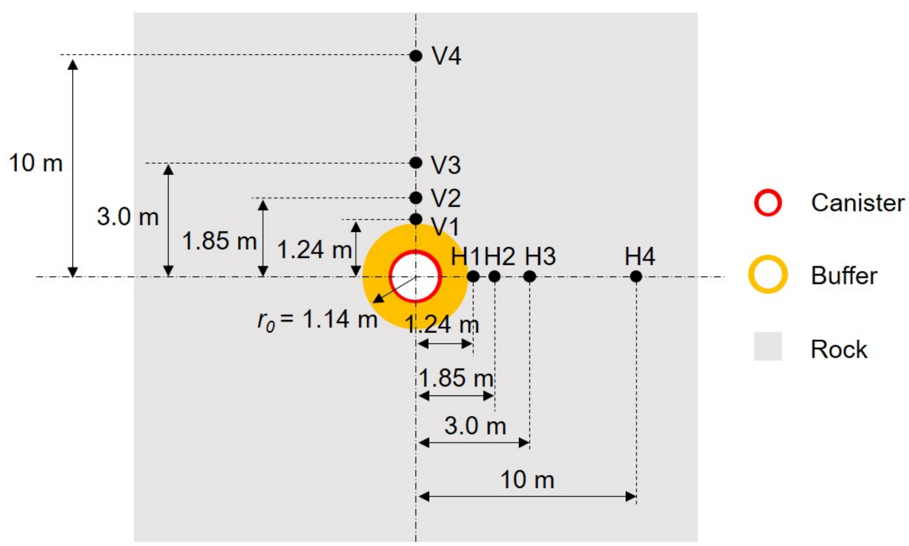

Figure 8 Locations in the rock where stress data are extracted for comparison.

Figure 9a and b show the evolution of the effective stresses in the rock during the canister heating stage for the isotropic and anisotropic rock stress cases, respectively. The in-plane shear stress change is not provided because its magnitude at these locations are found to be a couple of orders of magnitude smaller than that of the other stresses.

Excellent matches are achieved between the coupled THM simulation case and the developed stress approximation method in the TH simulation case, in both the isotropic and anisotropic rock stress cases. This shows the effectiveness of the developed stress approximation method to estimate stress changes in the rock in a geologic nuclear waste repository using only TH variables.

Largest errors are calculated at the location V1 and H1. For example, in the isotropic stress case, the largest error occurs in approximately two years since canister emplacement where -56%, 12% and 1% errors are generated in the radial, circumferential, and out-of-plane effective stress estimates, respectively, at both V1 and H1 locations. These errors correspond to errors in buffer stress estimates where mean total and mean net stresses are miscalculated by -73% and -87%, respectively. However, such errors diminish in 10 years, after which is more critical to PA and radionuclide transport than the earlier timeframe. Therefore, these errors are not significant.

The stresses are initially anisotropic near the tunnel for the isotropic rock stress case ($\sigma'_{rr} = 3$ MPa, $\sigma'_{yy} = 10$ MPa, $\sigma'_{\theta\theta} = 17$ MPa at location V1), whereas they are close to an isotropic stress state for the anisotropic rock stress case ($\sigma'_{rr} = 0.5$ MPa, $\sigma'_{yy} = 2$ MPa, $\sigma'_{\theta\theta} = 3$ MPa at location V1). This is induced by the cylindrical cavity contraction during the tunnel excavation stage; the tunnel wall relaxes toward the center of the tunnel during excavation, which reduces the radial effective stress, while at the same time increases the circumferential effective stress.

During the canister heating stage, on the other hand, the cavity expansion occurs as the bentonite buffer swells in the confined space in the tunnel. The cavity expansion, combined with thermal pressurization, causes a significant reduction in the circumferential effective stress level at the H1 location. The radial and out-of-plane effective stress levels are not affected significantly as cavity expansion increases the radial and out-of-plane total stress levels which compensates for the pore pressure buildup from thermal pressurization.

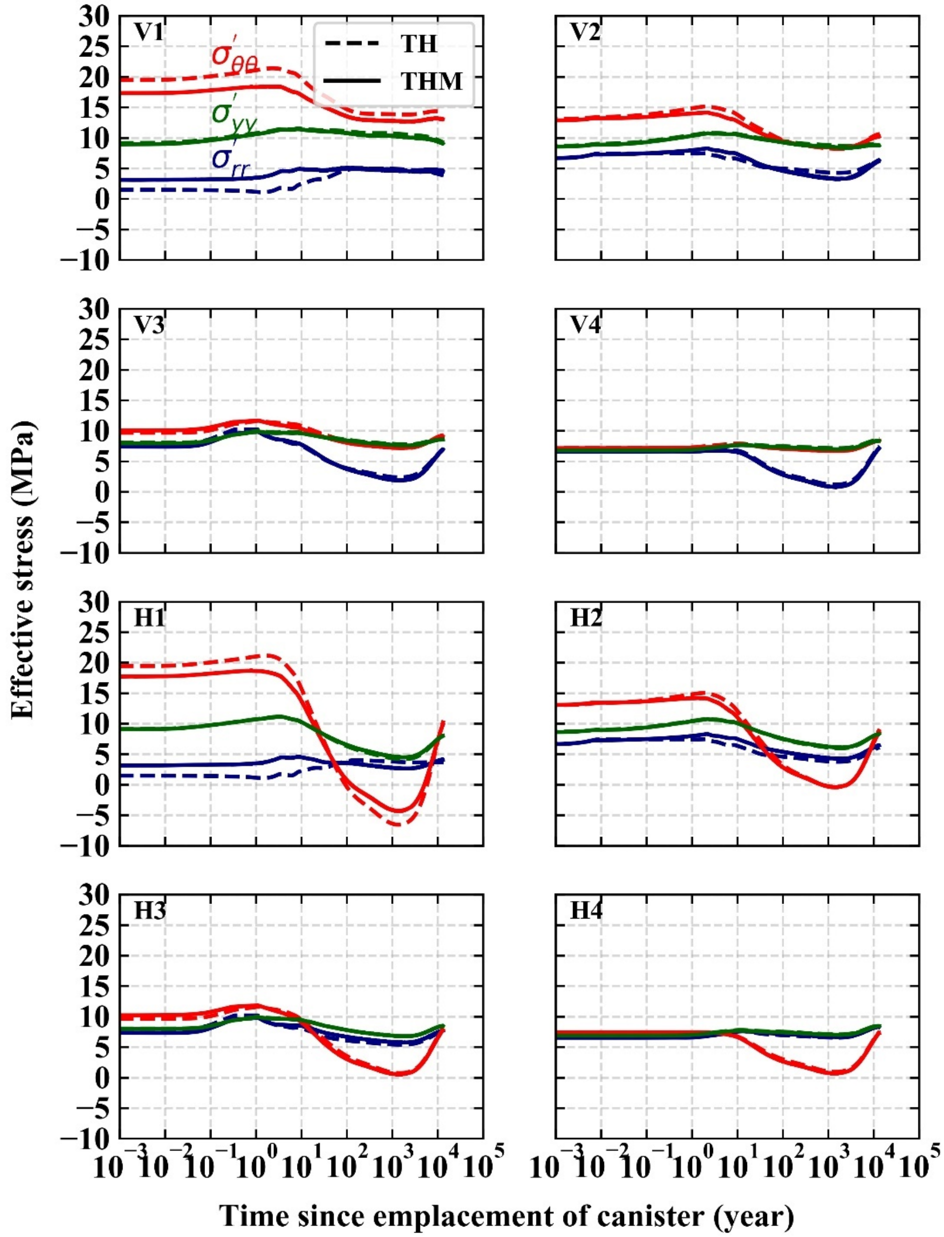
V1
V2
V3
V4
H1
H2
H3
H4
TH
THM
$\sigma'_{\theta\theta}$
σ'_{yy}
σ'_{rr}
Effective stress (MPa)
Time since emplacement of canister (year)
30
25
20
15
10
5
0
−5
−10
10^{-3} 10^{-2} 10^{-1} 10^{0} 10^{1} 10^{2} 10^{3} 10^{4} 10^{5}

(a)

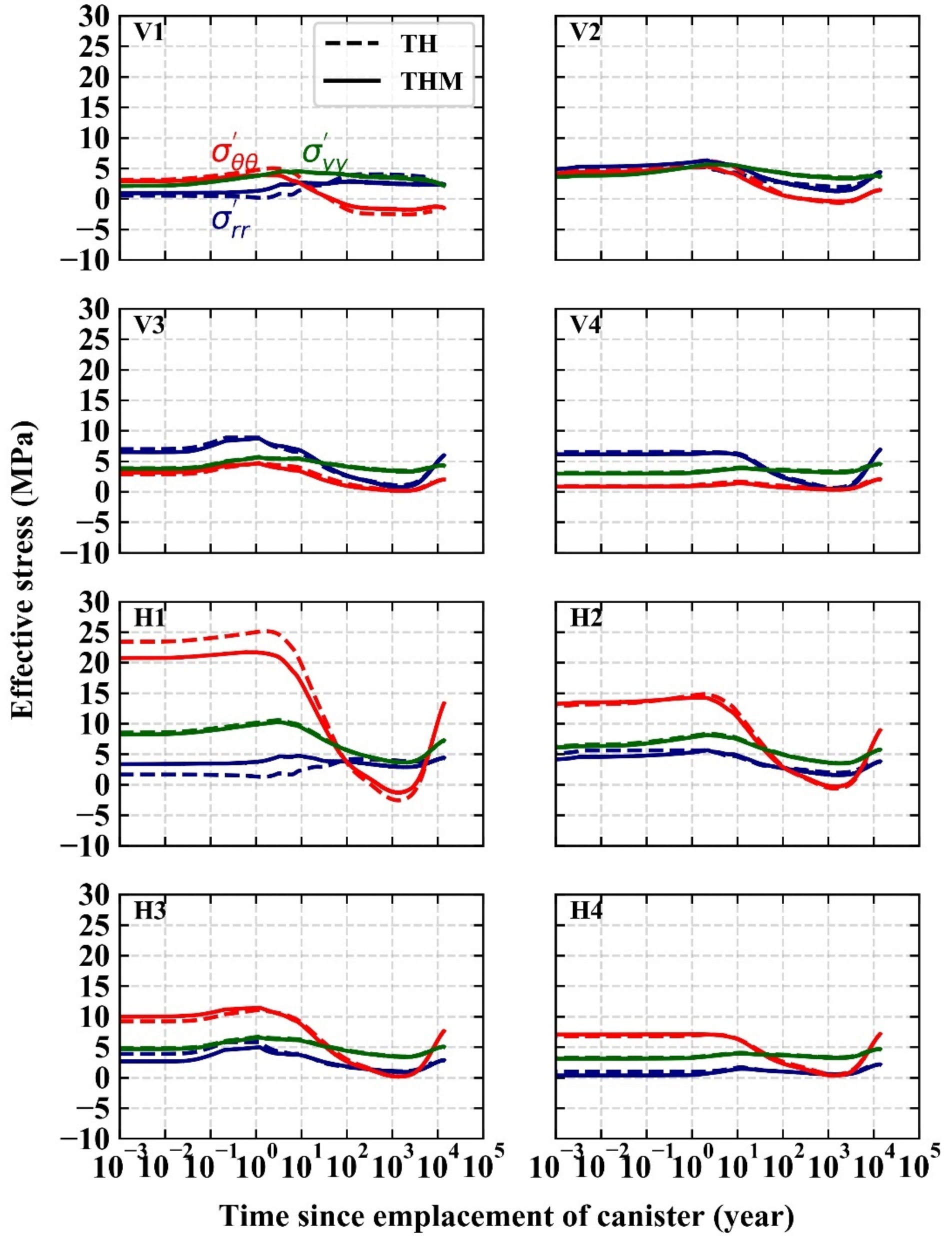

(b)

Figure 9 Effective stress changes in the rock near the tunnel during the canister heating stage: (a) isotropic rock stress case; (b) anisotropic rock stress case.

Figure 10a and b show the change in mean effective and deviatoric stresses during the canister heating stage for the isotropic and anisotropic rock stress cases, respectively. The match between the coupled THM simulation case and developed stress approximation method in the TH simulation case is excellent in both cases. The mean effective stress change in the TH case, for example, seems to match perfectly with that in the THM case at all examined locations in the rock, whereas greater errors are generated in the deviatoric stress change near the tunnel wall (location V1, V2, H1, H2). This is because errors in the radial, circumferential, and out-of-plane effective stresses are averaged out in the calculation of mean effective stress, whereas they are magnified in the calculation of deviatoric stress. Nevertheless, errors in the deviatoric stress change diminish in 10 years, and hence such errors at the early timeframe would not be critical for the long-term radionuclide transport.

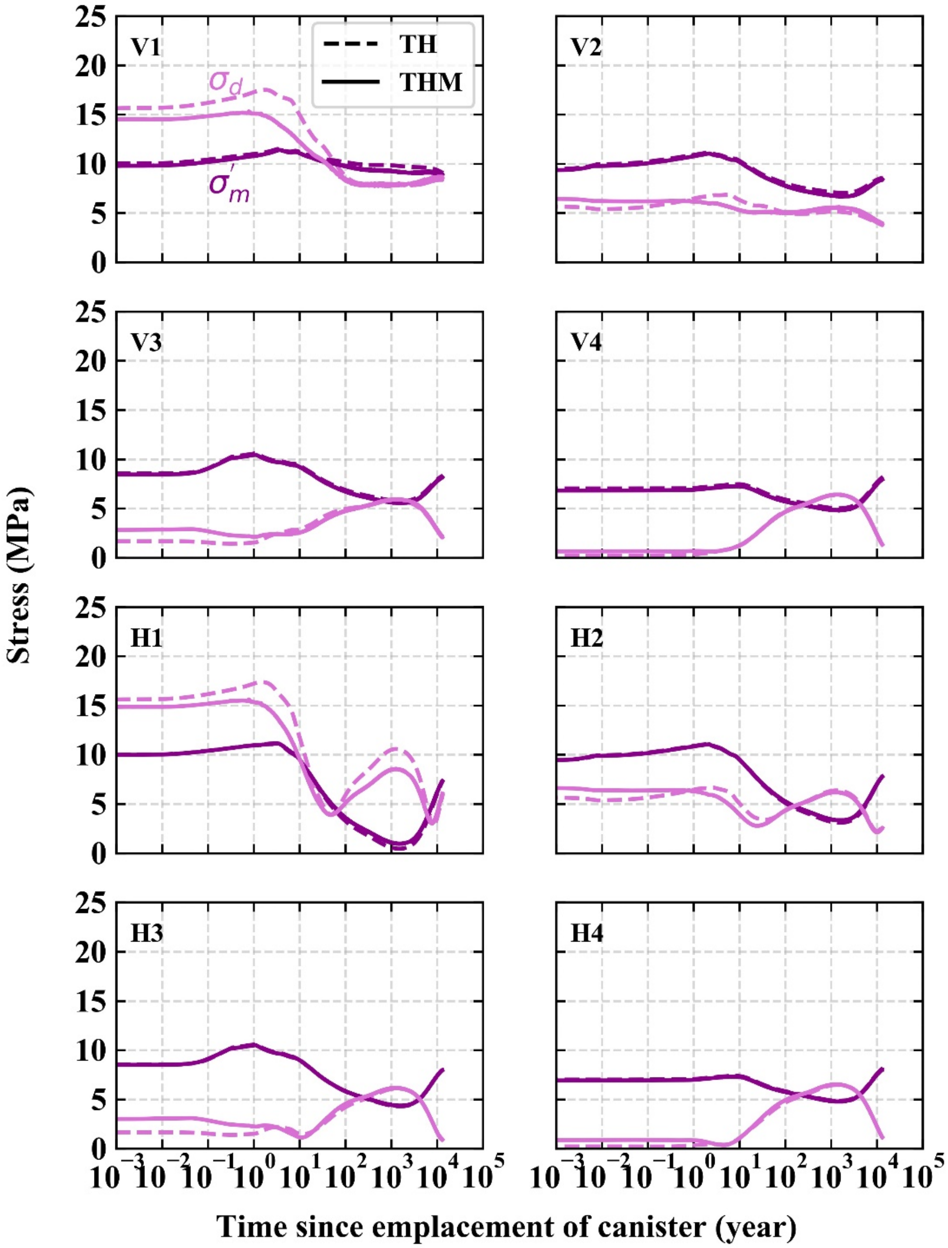
V1
V2
V3
V4
H1
H2
H3
H4
TH
THM
σ_d
σ_m'
Stress (MPa)
Time since emplacement of canister (year)

(a)

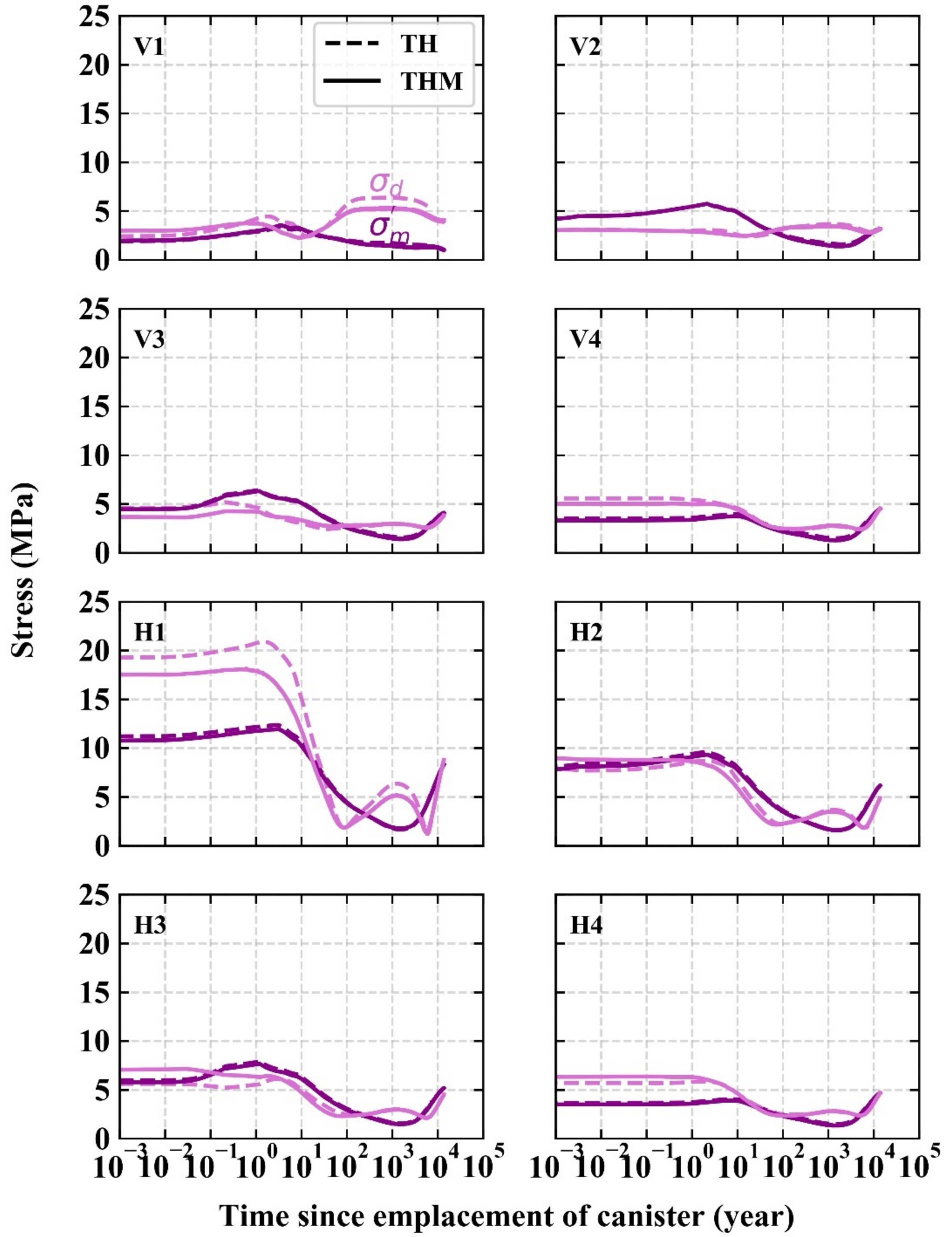

(b)

Figure 10 Mean effective and deviatoric stress changes in the rock near the tunnel during the canister heating stage: (a) isotropic rock stress case; (b) anisotropic rock stress case.

3.4 Rock permeability

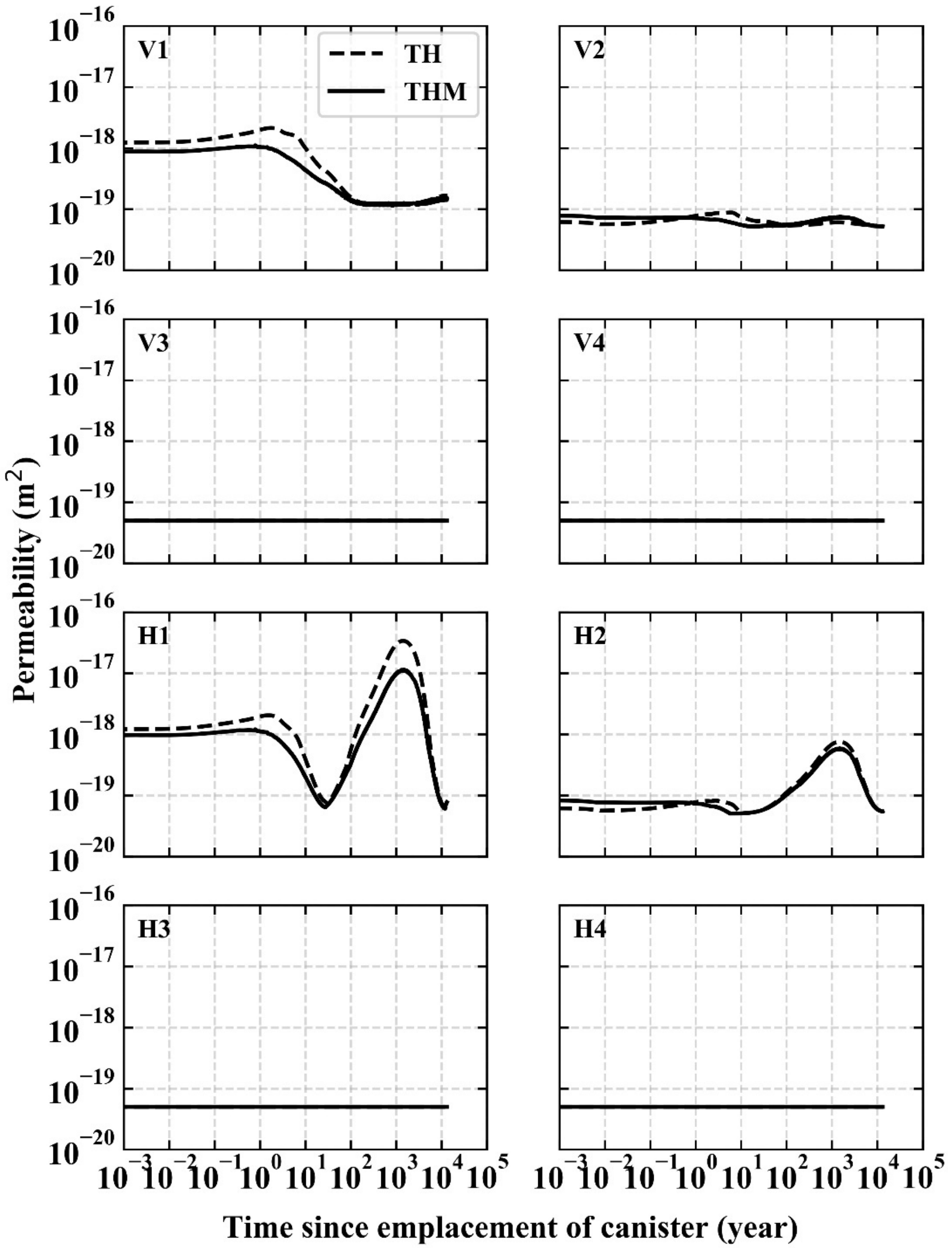

(a)

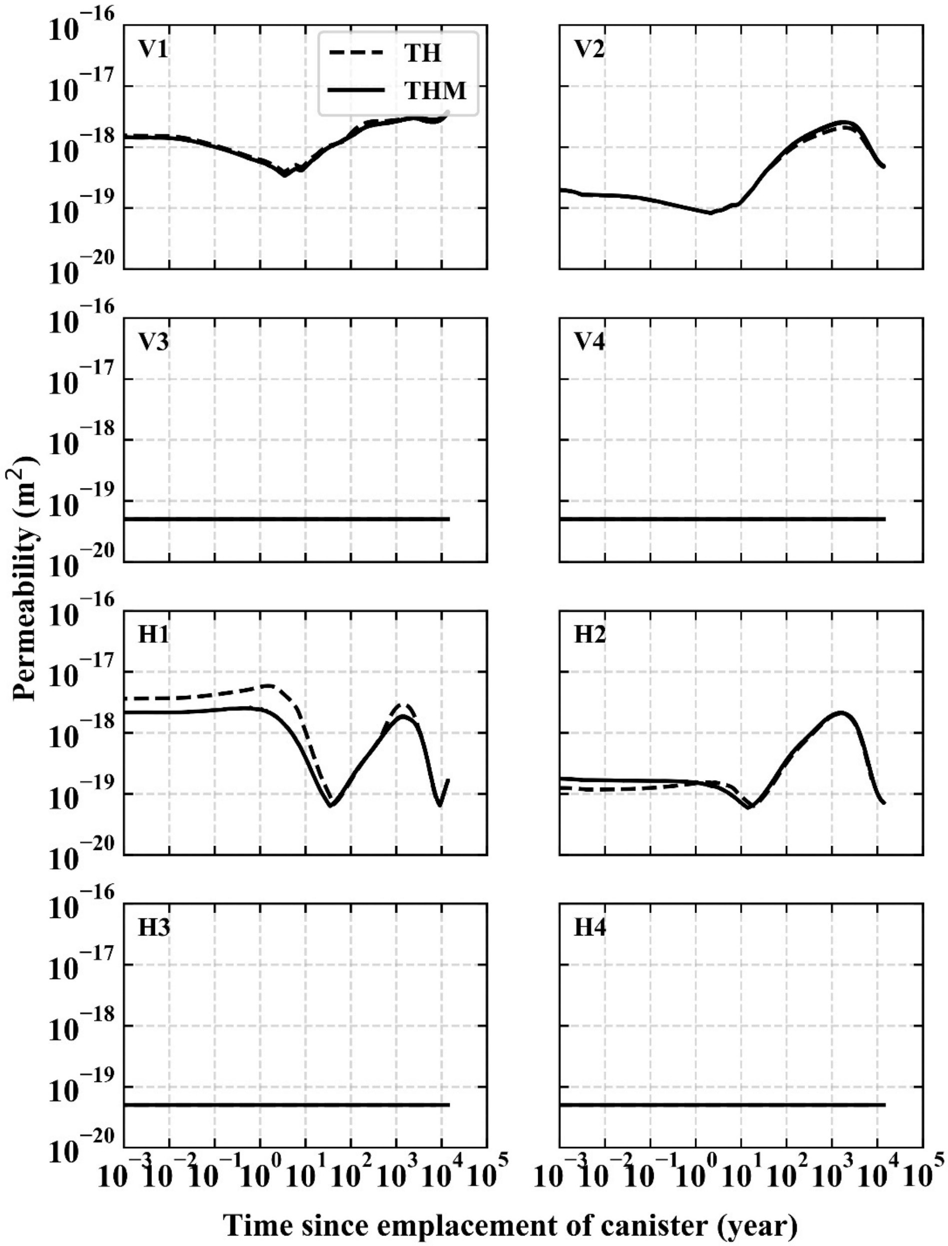

(b)

Figure 11 Absolute permeability changes in the rock near the during the canister heating stage: (a) isotropic rock stress case; (b) anisotropic rock stress case.

Figure 11a and b show stress-induced absolute permeability changes in the rock near the tunnel for the isotropic and anisotropic rock stress cases, respectively. Stress-induced permeability changes occur only at locations within the excavation damaged zone (V1, V2, H1, H2), which are defined as the area inside twice the radius of the tunnel in this study. At these locations, permeability values are calculated higher than the in situ rock permeability ($5 \cdot 10^{-20}$ m^2) due to stress-induced fracture opening.

The permeability value at the H1 location decreases initially by a couple of magnitudes (1-20 years) but it then increases by two orders of magnitude (20-1000 years) in the isotropic rock stress case. The initial permeability decrease is caused by the buffer swelling-induced pressure increase normal to the tunnel wall, which decreases the deviatoric stress level via cavity expansion, whereas the following permeability increase is due to the combination of thermal pressurization-induced mean effective stress decrease and further cavity expansion which increases the deviatoric stress level. Similar permeability changes occur in the anisotropic rock stress case according to the same mechanism at the H1 location.

At the V1 location, the permeability change is governed by the deviatoric stress change in the isotropic rock stress case, while it is controlled by the mean effective stress change in the anisotropic rock stress case. This is because the deviatoric stress level increases (from the initial zero value) and exceeds the critical level of 5 MPa after tunnel excavation in the isotropic stress case, whereas it decreases (from the initial nonzero value) and drops below the critical level in the anisotropic stress case. As a result, thermal pressurization-induced mean effective stress is more critical to the permeability change in the anisotropic rock stress case than in the isotropic case at the V1 location.

The match in rock permeability between the THM simulation and developed TH stress approximation method is found adequate, as relatively large errors of over 100% are generated near the tunnel wall in the horizontal direction (i.e., location H1) at approximately 2 years since canister emplacement. The error is caused by the overestimation of the deviatoric stress in the developed TH method. The permeability function employed in this study (Equation 33) is an exponential function of deviatoric stress above the critical value (5 MPa in this study), hence errors in deviatoric stress estimate above 5 MPa are exponentially magnified in the permeability calculation. These errors, however, are not critical as they diminish in roughly 10 years, after which is the target timeframe for long-term PA and radionuclide transport simulations. Also, these errors are still small compared to the change in the permeability level during the canister heating stage, which is a couple of orders of magnitude.

4. Discussion

Errors in the permeability estimate have been shown insignificant in the previous section, but such errors will be affected by specific parameter values (Table 3) of the function employed in this study (Equation 33) and by the permeability function itself. Therefore, further studies are necessary to evaluate the effect of different permeability functions (such as Li & Liu, 2013; Rutqvist & Tsang, 2003) on the accuracy of the permeability change estimated by the developed TH stress approximation method.

The excavation damaged zone (EDZ) is assumed to remain constant in this study. This might not be appropriate as the calculated deviatoric stress levels outside the EDZ (locations V3, V4, H3, H4) tend to increase significantly in a later timeframe (~1,000 years) during the canister heating stage (Figure 10). This deviatoric stress increase may cause shear fracture development outside the EDZ and hence the permeability profile around the tunnel may be altered. Tensile fracture, on the other hand, would be unlikely to develop outside the EDZ as the calculated effective stresses tend to remain in compression (Figure 9).

Also, the host rock formation is assumed a linear elastic material in this study. The actual formation, especially in the EDZ, may exhibit plastic and visco-elastic (creep) behaviors, which could affect the stress profile around the tunnel significantly. The modelling of such plastic and visco-elastic rock behaviors is outside the scope of this study, and hence it may be addressed in future studies. This may also include longer-term healing and sealing created fractures in the EDZ, whose occurrence will depend on the site-specific host rock properties. The approach developed and tested in this study, which should involve calibration and validation of the stress-permeability function against site specific field experiments, is a way to implicitly consider these effects in the simplified elastic model simulations.

5. Conclusions

In this study, a coupled THM simulation of the long-term behavior of a generic nuclear waste repository in clay/shale formation has been conducted, in order to estimate stress and stress-induced permeability change in the formation around the disposal tunnel. A methodology has been developed for approximating the stress and stress-induced permeability change by using only TH variables, in order to facilitate the incorporation of stress-induced permeability change into existing TH simulators for radionuclide transport simulations in the PA of a repository site. The TOUGH-FLAC simulator was used to model the coupled THM response of the entire repository during canister heating while Barcelona Basic Model (BBM) is employed to model the mechanical behavior of swelling bentonite buffer. Results have provided the following findings:

- Absolute permeability in clay/shale formation in the proximity of the disposal tunnel could change by two orders of magnitude due to stress-induced fracture opening and closing during the first 10,000 years of geologic disposal.

- Stress and stress-induced permeability change estimated by the developed stress approximation methodology in the TH simulation match those calculated by the coupled THM simulation.
- The maximum error in the permeability estimate is found to be a fraction of the range of calculated permeability change, which is a couple of orders of magnitude.
- Such errors are found to diminish in 10 years since the canister emplacement and the match in the long term is found to be excellent.

Therefore, the accuracy of the developed stress approximation methodology in estimating stress and stress-induced permeability change has been shown adequate. Future studies mentioned in the preceding section will improve the accuracy and reliability of the developed methodology so as to increase the confidence in applying it for the PA and radionuclide transport simulations.

Acknowledgment

Funding was provided by the Spent Fuel and Waste Science and Technology, Office of Nuclear Energy, of the U.S. Department of Energy under Contract Number DE-AC02-05CH11231 with Lawrence Berkeley National Laboratory.

References

[1] D. Vinson and C. J.T., “Spent Nuclear Fuel and High-Level Radioactive Waste Inventory Report. U.S. Department of Energy, Spent Fuel and Waste Disposition. FCRD-NFST-2013-000263, Rev. 6,” 2019.

[2] M. E. Kraft, “Nuclear power and the challenge of high-level waste disposal in the United States,” *Polity*, vol. 45, no. 2, pp. 265–280, 2013, doi: 10.1057/pol.2013.4.

[3] B. Faybishenko, J. Birkholzer, D. Sassani, and S. P., “International Approaches for Nuclear Waste Disposal in Geological Formations: Geological Challenges in Radioactive Waste Isolation—Fifth Worldwide Review. Prepared for the U.S. Department of Energy Spent Fuel and Waste Science and Technology R&D Campaign,” 2016.

[4] G. S. Bodvarsson, W. Boyle, R. Patterson, and D. Williams, “Overview of scientific investigations at Yucca Mountain—the potential repository for high-level nuclear waste,” *J. Contam. Hydrol.*, vol. 38, no. 1–3, pp. 3–24, 1999, doi: 10.1016/S0169-7722(99)00009-1.

[5] IAEA, “Scientific and Technical Basis for the Geological Disposal of Radioactive Wastes, Technical Report Series No. 413,” Vienna, 2003.

[6] IAEA, “Spent Fuel and High Level Waste: Chemical Durability and Performance under Simulated Repository Conditions,” Vienna, 2007.

[7] O. Fouché, H. Wright, J.-M. Le Cléac’h, and P. Pellenard, “Fabric control on strain and rupture of heterogeneous shale samples by using a non-conventional mechanical test,” *Appl. Clay Sci.*, vol. 26, no. 1–4, pp. 367–387, 2004, doi: 10.1016/j.clay.2003.12.014.

[8] D. Patriarche, E. Ledoux, R. Simon-Coinçon, J.-L. Michelot, and J. Cabrera, “Characterization and modeling of diffusion process for mass transport through the Tournemire argillites (Aveyron, France),” *Appl. Clay Sci.*, vol. 26, no. 1–4, pp. 109–122, 2004, doi: 10.1016/j.clay.2003.10.005.

[9] P. Meier, T. Trick, P. Blumling, and G. Volckaert, “Self-healing of fractures within the EDZ at the Mont Terri Rock Laboratory: results after one year of experimental work,” in *Proceedings of the*

international workshop on geomechanics, hydromechanical and thermomechanical behavior of deep argillaceous rocks: theory and experiments, 2000.

[10] J. D. Barnichon and G. Volckaert, “Observations and predictions of hydromechanical coupling effects in the Boom clay, Mol Underground Research Laboratory, Belgium,” *Hydrogeol. J.*, vol. 11, no. 1, pp. 193–202, 2003, doi: 10.1007/s10040-002-0240-6.

[11] S. Gonzales and K. S. Johnson, “Shales and other argillaceous strata in the United States,” Athens, GA (USA), 1985.

[12] F. D. Hansen *et al.*, “Shale Disposal of U . S . High-Level Radioactive Waste,” Albuquerque, New Mexico, 2010.

[13] P. Dobson and J. Houseworth, “Inventory of Shale Formations in the US, Including Geologic, Geochemical, Hydrological, Mechanical, and Thermal Characteristics. Prepared for U.S. Department of Energy, Used Fuel Disposition Campaign, FCRD-UFD-2014-000512,” 2013.

[14] P. . Mariner *et al.*, “Progress in Deep Geologic Disposal Safety Assessment in the U.S. since 2010. Prepared for U.S. Department of Energy, Spent Fuel and Waste Disposition. M2SF-19SN010304041, SAND2019-12001 R,” 2019.

[15] G. E. Hammond, P. C. Lichtner, and R. T. Mills, “Evaluating the performance of parallel subsurface simulators: An illustrative example with PFLOTRAN,” *Water Resour. Res.*, vol. 50, no. 1, pp. 208–228, 2014, doi: 10.1002/2012WR013483.

[16] G. Chen, X. Sillen, J. Verstricht, and X. Li, “ATLAS III in situ heating test in boom clay: Field data, observation and interpretation,” *Comput. Geotech.*, vol. 38, no. 5, pp. 683–696, 2011, doi: 10.1016/j.compgeo.2011.04.001.

[17] B. François, L. Laloui, and C. Laurent, “Thermo-hydro-mechanical simulation of ATLAS in situ large scale test in Boom Clay,” *Comput. Geotech.*, vol. 36, no. 4, pp. 626–640, 2009, doi: 10.1016/j.compgeo.2008.09.004.

[18] G. Armand, F. Bumbieler, N. Conil, de la V. R., J.-M. Bosgiraud, and M.-N. Vu, “Main outcomes from in situ thermo-hydro-mechanical experiments programme to demonstrate feasibility of

radioactive high-level waste disposal in the Callovo-Oxfordian claystone," *J. Rock Mech. Geotech. Eng.*, vol. 9, no. 3, pp. 415–427, 2017, doi: 10.1016/j.jrmge.2017.03.004.

[19] J. Rutqvist, L. Zheng, F. Chen, H. H. Liu, and J. Birkholzer, "Modeling of coupled thermo-hydro-mechanical processes with links to geochemistry associated with bentonite-backfilled repository tunnels in clay formations," *Rock Mech. Rock Eng.*, vol. 47, no. 1, pp. 167–186, 2014, doi: 10.1007/s00603-013-0375-x.

[20] L. Zheng, J. Rutqvist, J. T. Birkholzer, and H. H. Liu, "Coupled THMC models for bentonite in an argillite repository for nuclear waste: illitization and its effect on swelling stress under high temperature," *Eng. Geol.*, vol. 230, pp. 118–129, 2017, doi: 10.1016/j.enggeo.2017.10.002.

[21] L. Zheng, J. Rutqvist, J. T. Birkholzer, and H. H. Liu, "On the impact of temperatures up to 200°C in clay repositories with bentonite engineer barrier systems: a study with coupled thermal, hydrological, chemical, and mechanical modeling," *Eng. Geol.*, vol. 197, pp. 278–295, 2015, doi: 10.1016/j.enggeo.2015.08.026.

[22] J. Rutqvist, "Thermal Management Associated with Geologic Disposal of Large Spent Nuclear Fuel Canisters in Tunnels with Thermally Engineered Backfill," *Tunn. Undergr. Sp. Technol.*, vol. 102, pp. 1–13, 2020, doi: 10.1016/j.tust.2020.103454.

[23] C. F. Tsang, F. Bernier, and C. Davies, "Geohydromechanical processes in the Excavation Damaged Zone in crystalline rock, rock salt, and indurated and plastic clays - In the context of radioactive waste disposal," *Int. J. Rock Mech. Min. Sci.*, vol. 42, no. 1, pp. 109–125, 2005, doi: 10.1016/j.ijrmms.2004.08.003.

[24] K. Luu, "TOUGH3-FLAC for Dummies," Berkeley, CA, 2020.

[25] Y. Jung, G. Shu Heng Pau, S. Finsterle, and C. Doughty, "TOUGH3 User's Guide," Berkeley, CA, 2018.

[26] Itasca Consulting Group, "FLAC3D — Fast Lagrangian Analysis of Continua in Three-Dimensions, Ver. 7.0," Minneapolis, 2020.

[27] J. Kim, H. A. Tchelepi, and R. Juanes, "Stability and convergence of sequential methods for

coupled flow and geomechanicas: fixed-stress and fixed-strain splits," *Comput. Methods Appl. Mech. Eng.*, vol. 200, no. 13–16, pp. 1591–1606, 2011, doi: 10.1016/j.cma.2010.12.022.

[28] L. Blanco-Martín, R. Wolters, J. Rutqvist, K. H. Lux, and J. T. Birkholzer, "Thermal-hydraulic-mechanical modeling of a large-scale heater test to investigate rock salt and crushed salt behavior under repository conditions for heat-generating nuclear waste," *Comput. Geotech.*, vol. 77, pp. 120–133, 2016, doi: 10.1016/j.compgeo.2016.04.008.

[29] J. Rutqvist, Y.-S. Wu, C.-F. Tsang, and G. Bodvarsson, "A modeling approach for analysis of coupled multiphase fluid flow, heat transfer, anddeformation in fracturedporous rock," *Int. J. Rock Mech. Min. Sci.*, vol. 39, no. 4, pp. 429–442, 2002, doi: 10.1016/S1365-1609(02)00022-9.

[30] J. Rutqvist, "Status of the TOUGH-FLAC simulator and recent applications related to coupled fluid flow and crustal deformations," *Comput. Geosci.*, vol. 37, no. 6, pp. 739–750, 2011, doi: 10.1016/j.cageo.2010.08.006.

[31] E. E. Alonso, A. Gens, and A. Josa, "A constitutive model for partially saturated soils," *Géotechnique*, vol. 40, no. 3, pp. 405–430, 1990, doi: 10.1680/geot.1991.41.2.273.

[32] M. T. van Genuchten, "A Closed-form Equation for Predicting the Hydraulic Conductivity of Unsaturated Soils1," *Soil Science Society of America Journal*, vol. 44, no. 5. p. 892, 1980, doi: 10.2136/sssaj1980.03615995004400050002x.

[33] E. E. Alonso, J. Vaunat, and A. Gens, "Modelling the mechanical behaviour of expansive clays," *Eng. Geol.*, vol. 54, no. 1–2, pp. 173–183, 1999, doi: 10.1016/S0013-7952(99)00079-4.

[34] M. Sánchez, A. Gens, L. do Nascimento Guimarães, and S. Olivella, "A double structure generalized plasticity model for expansive materials," *Int. J. Numer. Anal. Methods Geomech.*, vol. 29, no. 8, pp. 751–787, 2005, doi: 10.1002/nag.434.

[35] P. Bossart, P. M. Meier, A. Moeri, T. Trick, and J. C. Mayor, "Geological and hydraulic characterisation of the excavation disturbed zone in the Opalinus Clay of the Mont Terri Rock Laboratory," *Eng. Geol.*, vol. 66, no. 1–2, pp. 19–38, 2002, doi: 10.1016/S0013-7952(01)00140-5.

[36] A. G. Corkum and C. D. Martin, "The mechanical behaviour of weak mudstone (Opalinus Clay) at

low stresses," *Int. J. Rock Mech. Min. Sci.*, vol. 44, no. 2, pp. 196–209, 2007, doi: 10.1016/j.ijrmms.2006.06.004.

[37] C. D. Martin and G. W. Lanyon, "Measurement of in-situ stress in weak rocks at Mont Terri Rock Laboratory, Switzerland," *Int. J. Rock Mech. Min. Sci.*, vol. 40, no. 7–8, pp. 1077–1088, 2003, doi: 10.1016/S1365-1609(03)00113-8.

[38] L. C. Li and H. H. Liu, "A numerical study of the mechanical response to excavation and ventilation around tunnels in clay rocks," *Int. J. Rock Mech. Min. Sci.*, vol. 59, pp. 22–32, 2013, doi: 10.1016/j.ijrmms.2012.11.005.

[39] J. Rutqvist and C. F. Tsang, "Analysis of thermal-hydrologic-mechanical behavior near an emplacement drift at Yucca Mountain," *J. Contam. Hydrol.*, vol. 62–63, pp. 637–652, 2003, doi: 10.1016/S0169-7722(02)00184-5.